# Power scalable 30-W mid-infrared fluoride fiber amplifier

HIYORI UEHARA,[1,3,*] DAISUKE KONISHI,[2] KENJI GOYA,[1,4] RYO SAHARA,[2] MASANAO MURAKAMI,[2] AND SHIGEKI TOKITA[1,*]

[1]*Institute of Laser Engineering, Osaka University, 2-6 Yamada-oka, Suita, Osaka 565-0871, Japan*
[2]*Mitsuboshi Diamond Industrial Co., Ltd., 32-12 Koroen, Settsu, Osaka 566-0034, Japan*
[3]*Currently with National Institutes of Natural Sciences, National Institute for Fusion Science, 322-6 Oroshi-cho, Toki, Gifu 509-5292, Japan*
[4]*Currently with Akita Prefectural University, 84-4 Ebinokuchi Tsuchiya, Yurihonjo, Akita 015-0055, Japan*
**Corresponding author: uehara.hiyori@nifs.ac.jp; tokita-s@ile.osaka-u.ac.jp*

Received XX Month XXXX; revised XX Month, XXXX; accepted XX Month XXXX; posted XX Month XXXX (Doc. ID XXXXX); published XX Month XXXX

**A fluoride-fiber-based master oscillator power amplifier for 30-W class continuous wave operation at 2.8-μm wavelength has been demonstrated. To overcome the low durability of ZBLAN fibers, various novel technologies for using fluoride glass with a ZBLAN-fiber-based side-pump combiner have been adopted in the system. A maximum cw output power of 33 W and stable operation under 23-W output have been demonstrated. We suggest that such fiber MOPA systems will open up advanced fluoride fiber technology for next-generation high-power mid-IR lasers.** 

http://dx.doi.org/10.1364/OL.99.099999

Recently, high-power mid-infrared lasers have attracted considerable attention. Because of their specific absorption properties by -OH bonds, high-average-power lasers around 3-μm wavelength are in demand for various applications in medicine [1] and remote sensing [2], as well as industrial applications, such as the processing of glass [3] and plastic materials [4] derived from thermal accumulation. 3-μm coherent sources can be achieved by various techniques, e.g. wavelength conversion [5], quantum cascade lasers [6], supercontinuum generation [7], Cr:ZnSe lasers [8] and Er-doped lasers [9-12]. Er-doped fluoride fibers whose qualities have improved over recent decades have been used in high-average-power lasers at 2.8 μm, and their output power is increasing [13-16]. Fluoride glass exhibiting low-phonon energies are one of the most suitable host materials for mid-IR lasers longer than 2-μm wavelength. However, fluoride glass has disadvantages, such as low mechanical strength and low heat resistance due to its lower thermal conductivity, lower melting temperature and higher hygroscopicity compared to silica glass or other single crystals. The heat generation ratio of 3-μm fluoride glass fiber laser reaches 40% [17] for a 0.97-μm excitation wavelength, which is much larger than that of a 1-μm fiber laser system. Although high-power pumping is required to obtain higher gain, powerful pumping from the fiber-end into a short-length fluoride fiber results in breakdown of the laser system due to overheating. A long-length fiber structure with attached multiple "side-pump combiners" is effective in overcoming the thermal problems, enabling homogeneous excitation of the whole fiber, which relieves thermal loading. The development of such fluoride-fiber-based devices including side-pump combiners has been challenging due to the significant fragility in the mechanical and chemical strength of fluoride fiber. The present record for a 2.8-μm continuous wave output power is 42 W, demonstrated by Aydin et al. [18] using an end-pumped $ZrF_4$-based fluoride (ZBLAN) fiber. However, their output power stability was limited under high-power operation over 20 W due to chemical interactions with ambient OH molecules at the fiber tips [18, 19]. Other problems of wavelength stability [18, 20] due to thermal effects also have to be taken into account even in wavelength-stabilized lasers using fiber Bragg gratings (FBGs). A master oscillator power amplifier (MOPA) system using a highly stable oscillator is an effective solution to the problems of fluoride glass fiber lasers described above. The MOPA structure enable the attainment of stabilized high-power lasers in output power, emission wavelength and beam quality. Recently, amplifier designs have been reported for cw [21] and pulsed [22, 23] Er:ZBLAN fiber lasers. Although side pumping would benefit such applications, the active fiber is still end pumped by a laser diode (LD), and the seed light is injected via a dichroic mirror into the amplifying fiber.

Last year, we reported the first fluoride-fiber-based pump combiner, fabricated by fusion splicing [24], with a view to constructing a side-pumped Er:ZBLAN fiber MOPA system for high-power operation. By using the pump combiners, 21-W cw oscillation was performed, although the MOPA system was not demonstrated at that time. In this work, we obtained a cw amplified output by a Er:ZBLAN fiber MOPA system at 2.8-μm using the side-pump combiners for the first time.

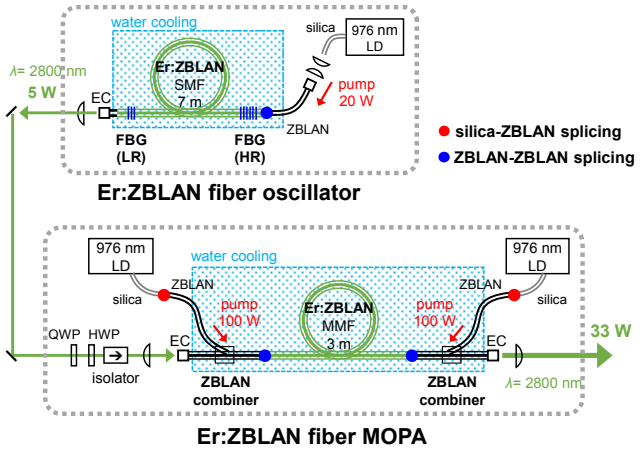


Fig. 1. Schematic diagram of the setup for an Er:ZBLAN fiber MOPA.

Figure 1 shows the experimental setup for a 2.8-μm MOPA system. The ZBLAN fibers used in the present study were purchased from FiberLabs, Inc. Double-clad active fiber, which has a 6-mol% Er-doped core of 15-μm diameter, 0.12 NA and a square-shaped first cladding 240 μm a side, were spliced with an undoped ZBLAN guide fiber with a core diameter of 280 μm. The optical coupling loss at the splicing portion is less than 0.05 dB. Fiber coupled 976-nm-stabilized LDs (K976AAHRN-27.00W, BWT) with a core diameter of 105 μm were coupled to the guide fiber via free-space. Two FBGs with high-reflectance (HR) and low-reflectance (LR) were fabricated on both sides of an active fiber by plane-by-plane inscription using a 513 nm femtosecond laser, as shown in Fig. 2(a), with a central Bragg wavelength of 2801 nm where atmospheric absorption is relatively low. Detailed information about the fabrication technique and optical properties of the FBG were reported in our previous paper [20]. The reflectivities of HR and LR-FBGs are 97% and 10-15%, respectively. The distance between the HR-FBG and the active fiber tip were shortened to less than 10 mm to reduce the absorption loss of the pump light and also inhibit parasitic oscillation. The output side of the active fiber was spliced with a 0.3-mm-length ZBLAN fiber spacer and an end-cap (EC) composed of $CaF_2$ single crystal of 1-mm-cubic to protect the fluoride fiber tip from OH diffusion. Such an EC protection enables long-term laser operation at 2.8 μm [25], because the $CaF_2$ crystal exhibits a higher thermal conductivity of 9.7 W/mK compared to $AlF_3$-based fluoride glass, which is generally used as EC material [17]. Recently, photodegradation effect on fiber tips in the 2.8 μm Er:ZBLAN oscillators were evaluated in detail by Aydin et al. [26] using various endcap materials. According to the ref. [26], stable cw operation over 100 hours was demonstrated under 20 W output by sputtering silicon nitride film on the output surface of the endcap. In our system, the difference of the refractive indices and thermal expansion coefficient between ZBLAN and $CaF_2$ is very small, which results in low Fresnel loss (<0.1%) and low residual stress after thermal splicing. The whole active fiber and FBGs were mounted on an aluminum plate, which was actively cooled with 20°C water, as shown by the blue-hatching in Fig. 1.

The MOPA part consists of several free-space optical elements and a bidirectional LD-side-pumped ZBLAN fiber amplifier including ZBLAN-based pump combiners. The output signal from the oscillator was polarization-controlled and isolated using two wave plates and a Faraday isolator. It was then coupled to the LP01 mode in a multi-mode ZBLAN fiber-core of 24 μm in mode-field diameter by observing a Gaussian-like beam pattern at another side of the amplifying fiber. Coupling efficiency over 95% was achieved by choosing such a larger core fiber. The incident signal power is about 52% of its power at the output of the oscillator. The side pump combiner shown in Fig. 2(b) consist of a double-clad multi-mode ZBLAN fiber (signal fiber) with a core of 28-μm diameter, 0.12 NA and a square-shaped first cladding with 240 μm a side, and a ZBLAN pump fiber with a core diameter of 170 μm. The coupling efficiency from the pump fiber core to the first-cladding of the signal fiber was 83%. An angle-polished pump fiber was spliced with the square-shaped double clad fiber by scanning the $CO_2$ laser around the fiber surface. Detailed information about the fabrication technique of the combiner were reported in our previous paper [24], the first demonstration of a fluoride-fiber-based pump combiner. The other side of the pump fiber was spliced with a silica glass fiber, which was coupled with a 976-nm-stabilized pumping LD (K976AG1RN-100.0W, BWT). The fusion splicing techniques of silica-fluoride glass fiber, reported in Ref. [10, 27, 28], is effective for reducing the coupling loss of the pump source [18]. Figure 2(c) shows a typical microscope image of a silica-ZBLAN spliced fiber. A relatively high bonding strength between the silica and ZBLAN of 2 MPa was achieved owing to the tapered structure of the ZBLAN fiber whose tip overlaps the silica fiber tip. The optical coupling loss at the splicing point is less than 0.22 dB. The coupling efficiency from the ZBLAN to silica fiber is only 20%, which means that this splicing works like an isolator to protect the LDs, due partly to the mostly absorbed pump light in the 3-m double clad fiber. It also has a fairly low coupling efficiency of much less than 1% between the core-propagated laser mode to the pump fiber. The reason why this silica-ZBLAN fiber splicing technique was not used in the oscillator is that the splicing portion was damaged frequently. The 2.8-μm counter-output passed through the HR-FBG and reached over 250 mW under 5-W operation, which might induce overheating due to drastic absorption by the silica glass. In previous work, an Er-doped fiber was used as a signal fiber in the combiner and the fiber branch was damaged by the heating effect under 60–80-W pumping. An undoped-fiber-based combiner inhibits the thermal loading at the weak part around the fiber branch and enables further powerful pumping in the present system. These two undoped signal fibers, including the pump combiner, were core-to-core spliced with a 6-mol% Er-doped signal fiber with the same core/clad diameters. This active fiber is long enough at 3 m to absorb the 976-nm pump light. An optical microscope image of the core-to-core spliced ZBLAN fiber is shown in Fig. 2(d). The core position and axis are perfectly aligned and the coupling losses for core/clad propagation are less than 0.3 dB and 0.05 dB, respectively. Core-to-core splicing errors should be reduced, which will cause amplified signal loss resulting in a reduction of not only the MOPA output but also the damage threshold of the fluoride fiber derived from signal leakage. Such a high-quality core-to-core splicing technique might be helpful for recovering fluoride-fiber laser systems. Two ECs spliced with signal fibers were given a dielectric AR coating (LAYERTEC GmbH) for 2.8 μm to reduce the signal loss by Fresnel reflection and inhibit parasitic oscillation in the amplifier due to multiple reflection. The whole active fiber, including the core-to-core spliced parts and the pump combiners, was mounted on an aluminum plate, which was cooled with 20°C water, as shown by the blue-hatching in Fig. 1.

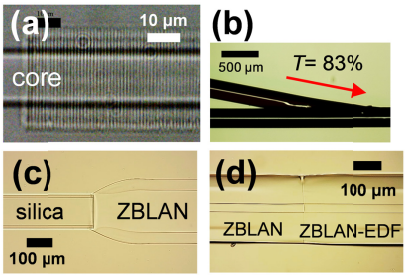


Fig. 2. Optical microscope images of (a) an FBG fabricated on an oscillator fiber core, (b) ZBLAN-fiber side pump combiner in the amplifier, (c) fusion spliced fiber between 125-μm silica fiber and 240-μm ZBLAN pump fiber in the amplifier, and (d) core-to-core spliced ZBLAN fiber between the undoped/Er-doped square-shaped double clad fibers with a core of 28 μm in diameter.

The output power of the oscillator is 5.0 W under 20-W pumping during this MOPA experiment. The pump threshold and slope efficiency are 2 W and 28%, respectively. The output power, beam profile and polarization state from the oscillator indicate long-term stability over 2000 hours under 5-W operation. The wavelength of the seed light from the oscillator was 2800.5 nm, which was in reasonable agreement with the Bragg wavelength of the FBGs. The input seed power on the front of the fiber amplifier was 2.6 W and the output power from the amplifier was 1.5 W without pumping. The transmission loss of the whole amplification fiber of 4.5-m length was 2.36 dB in the steady state. ZBLAN fiber propagation loss of 0.45 dB/m measured at 2.8 μm is included in this total loss. Figure 3(a) shows the amplified output power as a function of the total power of bidirectional pumping under 2.6-W input. The pump powers for co- and counter-propagating were always the same and the maximum pump power was 100 W at each LD. The maximum amplified output power was 33.1 W under 190-W pumping. To the best of our knowledge, this is the highest output power obtained by an Er:ZBLAN-fiber MOPA. The previous record was 4.6 W [21]. The amplification slope efficiencies in the ranges 0–100-W and 100–190-W pumping were 20% and 14%, respectively. One of the reasons for the degradation of efficiency, which was also observed in a previous report [24], is considered to be a gain reduction attributed to the temperature increase of the active fiber. The output spectra were measured for various pump powers by an optical spectrum analyzer (OSA205C, Thorlabs), shown in Fig. 3(b). The signal intensities are normalized and the parasitic oscillations generated by shutting off the seed light are plotted at the bottom of the figure for comparison. No spectral shift or parasitic oscillation, which should be obtained at 2780 to 2790 nm, were observed for the whole range of pumping power from 0 to 190 W. The laser wavelength of 2800.5 nm and its linewidth of less than 0.1 nm were identical with the seed laser even under 30-W operation. It is critically important that the MOPA regime was available without parasitic laser oscillation even under such a high-gain condition. The wavelength dependence of the Er-doped ZBLAN fiber MOPA have been discussed in reference [21]. Figure 4 shows the result of a laser beam diameter measurement and typical intensity profiles (inset) taken by a pyroelectric camera (Pyrocam III, Ophir) for (a) the oscillator output, (b) amplified output and (c) parasitic oscillation beam in the amplification fiber. The Gaussian beam quality factor of the oscillator output was calculated to be $M^2$ = 1.19 derived from a 15-μm core single-mode fiber of 2.0 in $V$-number. Note that the MOPA output keeps a nearly Gaussian beam with $M^2$ = 1.28–1.44, though the amplification fiber with a 28-μm core exhibited a multi-mode of 3.8 in $V$-number. It means that the seed light which was mostly coupled to LP01 mode was amplified absolutely. On the other hand, the beam profile of the parasitic oscillation was clearly affected by the multi-transverse-mode property inside the fiber and the quality was $M^2$ = 1.84–2.23.

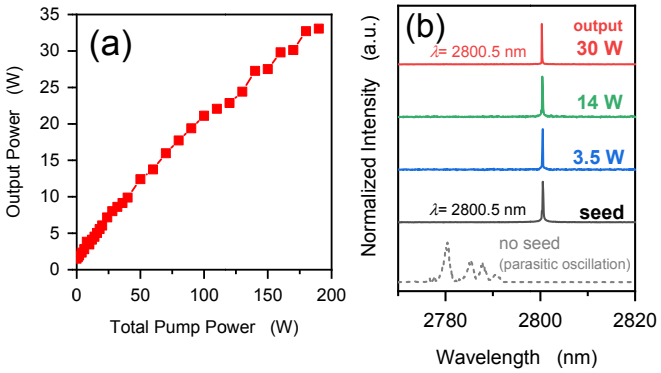


Fig. 3. (a) Amplified output power as a function of the total power of bidirectional pumping under 2.6-W input power. (b) Amplified output spectra at various pump powers. The signal intensities are normalized and the parasitic oscillation is plotted at the bottom for comparison.

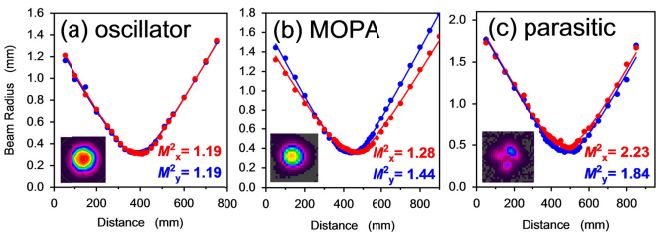


Fig. 4. Measured beam radius as a function of the beam propagation position for (a) the oscillator output, (b) amplified output and (c) parasitic oscillation beam. The inserted figures are the typical intensity profiles of the output beam.

The output power stabilities were observed using a thermopile power meter (L50A, Ophir) for output of 20 W, 23 W and 30 W, as shown in Fig. 5. For the 20-W and 23-W operation, the output power exhibited quite high stability with rms = 0.2–0.3% over a period of 60 minutes. Under 30-W operation, however, the power stability exhibited larger fluctuations and the MOPA fiber was damaged within 3 minutes. The damaged portion was around the core-to-core splicing of the output side, where the temperature of the undoped/Er-doped surface increases drastically due to the powerful pumping. Two likely reasons for this breakdown are core-damage due to localized heating or damage to the plastic-based second-cladding by leakage of the 2.8-μm signal. The nonlinear behavior of the input–output property above 28-W output power in Fig. 3(a) might be evidence of thermal loading. Note that no photodegradation was observed on the fiber tips after 30-W operation. For further power scaling in two combiners system, which may require a larger first-cladding design for the amplifier with a lower absorption coefficient and more effective

cooling system. As mentioned in the experimental session, the fiber branch suffered damage under 60–80-W pumping in our previous work [24] that is adopting Er-doped fiber in the combiner. Undoped signal fiber allows almost 100-W pumping for each combiner without breakdown in the present improved system. The power intensity at the fiber tip of the amplified output was estimated to be 7 MW/cm$^2$ under 33-W operation. This value is lower than the typical power density inside the cavity in a 10-W-level Er:ZBLAN fiber oscillator using a single-mode fiber. The MOPA system using a larger core fiber is suitable for high-power operation maintaining high stability of the output power, wavelength, and beam quality.

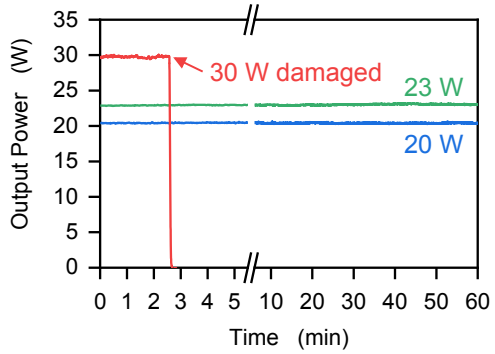


Fig. 5. Temporal output power stabilities of Er:ZBLAN fiber MOPA at output powers of 20 W, 23 W and 30 W continuously.

We propose the fiber MOPA system adopting our side-pump combiners and $Si_3N_4$ coated ECs [26] as a potential candidate high-average-power 3-μm source with industrial grade performance. This oscillator/amplifier-separated structure exhibits high maintainability, robustness and a small foot-print of 30 × 30 cm$^2$. Further power scaling will be realized by increasing the number of combiners and fiber length. The power amplification range was 32 W using a 3-m-long gain fiber with two combiners in the present system. A 100-W-level output is expected for a 9-m-long fiber and six combiners (total 550–600-W pumping), if the durability of each splicing portion will be improved in a future system. A powerful 3-μm source is suitable for pumping a Fe:ZnSe mid-IR laser [29], as an example of use. Various original techniques for the fluoride materials employed in this system, including side-pump combiners, make it possible to develop next-generation fluoride-material-based laser systems, not only Er-doped but also Dy-doped mid-IR lasers [30, 31]. In addition, diverse combinations with master oscillators e.g. Er:YAG [32], Er:$Lu_2O_3$ [33] and Cr:ZnSe [8], could be considered using an Er:ZBLAN fiber amplifier which exhibits a broadband gain property in the wavelength range 2700–2900-nm. We suggest that our fiber MOPA will lead the way to advanced fluoride fiber technologies for high-power mid-IR lasers.

**Funding.** We acknowledge funding from the "Adaptable and Seamless Technology Transfer Program through Target-driven R&D" (No. AS2716004) of the Japan Science and Technology Agency (JST) and a Kakenhi Grant-in-Aid (No. 18H01899) from the Japan Society for the Promotion of Science (JSPS) and grants from the Amada Foundation (Nos. AF-2017232, AF-2018228-C2 and AF-2018209-B2).

## References

1. J.-L. Boulnois, Lasers Med. Sci. **1**, 47 (1986).
2. P. Werle, F. Slemr, K. Maurer, R. Koormann, R. Mucke, and B. Janker, Opt. Lasers Eng. **37**, 101 (2002).
3. O. Y. F. Henry, S. A. Piletsky, and D. C. Cullen, Biosens. Bioelectron. **23**, 1769 (2008).
4. M. Murakami, C. Schaefer, S. Hattori, and K. Yahata, Proceedings of the 83rd Laser Materials Processing Conference, p. 117 (2015).
5. G. A. Rines, H. H. Zenzie, R. A. Schwarz, Y. Isyanove, and P. F. Moulton, IEEE J. Sel. Top. Quantum Electron. **1**, 50 (1995).
6. F. Capasso, R. Paiella, R. Martini, R. Colombelli, C. Gmachl, T. L. Myers, R. M. Williams, C. G. Bethea, K. Unterrainer, H. Y. Hwang, D. L. Sivco, A. Y. Cho, A. M. Sergent, H. C. Liu, and E. A. Whittaker, IEEE J. Quantum Electron. **38**, 511 (2002).
7. X. Guo, S. Tokita, K. Yoshii, H. Nishioka, and J. Kawanaka, Opt. Express **25**, 21171 (2017).
8. S. B. Mirov, I. S. Moskalev, S. Vasilyev, V. Smolski, V. V. Fedorov, D. Martyshkin, J. Peppers, M. Mirov, A. Dergachev, and V. Gapontsev, IEEE J. Sel. Top. Quantum Electron. **24**, 1601829 (2018).
9. S. D. Jackson, Nat. Photonics **6**, 423 (2012).
10. V. Fortin, M. Bernier, S. T. Bah, and R. Vallée, Opt. Lett. **40**, 2882 (2015).
11. H. Uehara, R. Yasuhara, S. Tokita, J. Kawanaka, M. Murakami, and S. Shimizu, Opt. Express **25**, 18677 (2017).
12. H. Kawase, and R. Yasuhara, Opt. Express **27**, 12213 (2019).
13. S. Tokita, M. Murakami, S. Shimizu, M. Hashida, and S. Sakabe, Opt. Lett. **34**, 3062 (2009).
14. X. Zhu and R. Jain, Opt. Lett. **32**, 26 (2007).
15. D. Faucher, M. Bernier, G. Androz, N. Caron, and R. Vallée, Opt. Lett. **36**, 1104 (2011).
16. Y. O. Aydın, V. Fortin, F. Maes, F. Jobin, S. D. Jackson, R. Vallée, and M. Bernier, Optica **4**, 235 (2017).
17. M. Pollnau, IEEE J. Quantum Electron. **39**, 350 (2003).
18. Y. O. Aydin, V. Fortin, R. Vallée, and M. Bernier, Opt. Lett. **43**, 4542 (2018).
19. N. Caron, M. Bernier, D. Faucher, and R. Vallée, Opt. Express **20**, 22188 (2012).
20. K. Goya, H. Matsukuma, H. Uehara, S. Hattori, C. A. Schäfer, D. Konishi, M. Murakami, and S. Tokita, Opt. Express **26**, 33305 (2018).
21. X. Zhu, and R. Jain, Opt. Lett. **33**, 1578 (2008).
22. G. Zhu, X. Zhu, R. A. Norwood, and N. Peyghambarian, Frontiers in Optics 2014, paper FW1D.2 (2014).
23. H. Luo, J. Li, J. Xie, B. Zhai, C. Wei, and Y. Liu, Opt. Express **24**, 29022 (2016).
24. C. A. Schäfer, H. Uehara, D. Konishi, S. Hattori, H. Matsukuma, M. Murakami, S. Shimizu, and S. Tokita, Opt. Lett. **43**, 2340 (2018).
25. S. Tokita, M. Murakami, and S. Shimizu, Advanced Solid State Lasers, paper AM3A.4 (2014).
26. Y. O. Aydin, F. Maes, V. Fortin, S. T. Bah, R. Vallée, and M. Bernier, Opt. Express **27**, 20659 (2019).
27. H. Okamoto, K. Kasuga, and Y. Kubota, Opt. Lett. **36**, 1470 (2011).
28. Z. Zheng, D. Ouyang, J. Zhao, S. Ruan, J. Yu, C. Guo, and J. Wang, Chin. Phys. Lett. **32**, 114206 (2015).
29. A. V. Pushkin, E. A. Migal, H. Uehara, K. Goya, S. Tokita, M. P. Frolov, Y. V. Korostelin, V. I. Kozlovsky, Y. K. Skasyrsky, and F. V. Potemkin, Opt. Lett. **43**, 5941 (2018).
30. R. I. Woodward, M. R. Majewski, G. Bharathan, D. D. Hudson, A. Fuerbach, and S. D. Jackson, Opt. Lett. **43**, 1471 (2018).
31. V. Fortin, F. Jobin, M. Larose, M. Bernier, and R. Vallée, Opt. Lett. **44**, 491 (2019).
32. D. W. Chen, C. L. Fincher, T. S. Rose, F. L. Vernon, and R. A. Fields, Opt. Lett. **24**, 385 (1999).
33. H. Uehara, S. Tokita, J. Kawanaka, D. Konishi, M. Murakami, S. Shimizu, and R. Yasuhara, Opt. Express **26**, 3497 (2018).

## Full References


1. J.-L. Boulnois, "Photophysical processes in recent medical laser developments: A review," Lasers Med. Sci. **1**(1), 47-66 (1986).
2. P. Werle, F. Slemr, K. Maurer, R. Koormann, R. Mucke, and B. Janker, "Near- and mid-infrared laser-optical sensors for gas analysis," Opt. Lasers Eng. **37**, 101-114 (2002).
3. O. Y. F. Henry, S. A. Piletsky, and D. C. Cullen, "Fabrication of molecularly imprinted polymer microarray on a chip by mid-infrared laser pulse initiated polymerization," Biosens. Bioelectron. **23**, 1769-1775 (2008).
4. M. Murakami, C. Schaefer, S. Hattori, and K. Yahata, Proceedings of the 83rd Laser Materials Processing Conference (Japan Laser Processing Society, 2015), p. 117.
5. G. A. Rines, H. H. Zenzie, R. A. Schwarz, Y. Isyanove, and P. F. Moulton, "Nonlinear conversion of Ti:sapphire laser wavelengths," IEEE J. Sel. Top. Quantum Electron. **1**(1), 50-57 (1995).
6. F. Capasso, R. Paiella, R. Martini, R. Colombelli, C. Gmachl, T. L. Myers, R. M. Williams, C. G. Bethea, K. Unterrainer, H. Y. Hwang, D. L. Sivco, A. Y. Cho, A. M. Sergent, H. C. Liu, and E. A. Whittaker, "Quantum cascade lasers: ultrahigh-speed operation, optical wireless communication, narrow linewidth, and far-infrared emission," IEEE J. Quantum Electron. **38**(6), 511-532 (2002).
7. X. Guo, S. Tokita, K. Yoshii, H. Nishioka, and J. Kawanaka, "Generation of 300 nm bandwidth 0.5 mJ pulses near 1 μm in a single stage gas filled hollow core fiber," Opt. Express **25**(18), 21171-21179 (2017).
8. S. B. Mirov, I. S. Moskalev, S. Vasilyev, V. Smolski, V. V. Fedorov, D. Martyshkin, J. Peppers, M. Mirov, A. Dergachev, and V. Gapontsev, "Frontiers of mid-IR lasers based on transition metal doped chalcogenides," IEEE J. Sel. Top. Quantum Electron. **24**(5), 1601829 (2018).
9. S. D. Jackson, "Towards high-power mid-infrared emission from a fibre laser," Nat. Photonics **6**, 423-431 (2012).
10. V. Fortin, M. Bernier, S. T. Bah, andR. Vallée, "30 W fluoride glass all-fiber laser at 2.94 μm," Opt. Lett. **40**(12), 2882-2885 (2015).
11. H. Uehara, R. Yasuhara, S. Tokita, J. Kawanaka, M. Murakami, and S. Shimizu, "Efficient continuous wave and quasi-continuous wave operation of a 2.8 μm Er:$Lu_2O_3$ ceramic laser," Opt. Express **25**(16), 18677-18684 (2017).
12. H. Kawase, and R. Yasuhara, "2.92-μm high-efficiency continuous-wave laser operation of diode-pumped Er:YAP crystal at room temperature," Opt. Express **27**(9), 12213-12220 (2019).
13. S. Tokita, M. Murakami, S. Shimizu, M. Hashida, and S. Sakabe, "Liquid-cooled 24 W mid-infrared Er:ZBLAN fiber laser," Opt. Lett. **34**(20), 3062-3064 (2009).
14. X. Zhu and R. Jain, "10-W-level diode-pumped compact 2.78 μm ZBLAN fiber laser," Opt. Lett. **32**(1), 26-28 (2007).
15. D. Faucher, M. Bernier, G. Androz, N. Caron, and R. Vallée, "20 W passively cooled single-mode all-fiber laser at 2.8 μm," Opt. Lett. **36**(7), 1104-1106 (2011).
16. Y. O. Aydın, V. Fortin, F. Maes, F. Jobin, S. D. Jackson, R. Vallée, and M. Bernier, "Diode-pumped mid-infrared fiber laser with 50% slope efficiency," Optica **4**(2), 235-238 (2017).
17. M. Pollnau, "Analysis of heat generation and thermal lensing in erbium 3-μm lasers," IEEE J. Quantum Electron. **39**(2), 350-357 (2003).
18. Y. O. Aydin, V. Fortin, R. Vallée, and M. Bernier, "Towards power scaling of 2.8 μm fiber lasers," Opt. Lett. **43**(18), 4542-4545 (2018).
19. N. Caron, M. Bernier, D. Faucher, and R. Vallée, "Understanding the fiber tip thermal runaway present in 3μm fluoride glass fiber lasers," Opt. Express **20**(20), 22188-22194 (2012).
20. K. Goya, H. Matsukuma, H. Uehara, S. Hattori, C. A. Schäfer, D. Konishi, M. Murakami, and S. Tokita, "Plane-by-plane femtosecond laser inscription of first-order fiber Bragg gratings in fluoride glass fiber for in situ monitoring of lasing evolution," Opt. Express **26**(25), 33305-33313 (2018).
21. X. Zhu, and R. Jain, "Watt-level Er-doped and Er–Pr-codoped ZBLAN fiber amplifiers at the 2.7–2.8 μm wavelength range," Opt. Lett. **33**(14), 1578-1580 (2008).
22. G. Zhu, X. Zhu, R. A. Norwood, and N. Peyghambarian, "Experimental and numerical investigations on 2.8 μm Q-switched pulse amplification," Frontiers in Optics 2014, paper FW1D.2 (2014).
23. H. Luo, J. Li, J. Xie, B. Zhai, C. Wei, and Y. Liu, "High average power and energy microsecond pulse generation from an erbium-doped fluoride fiber MOPA system," Opt. Express **24**(25), 29022-29032 (2016).
24. C. A. Schäfer, H. Uehara, D. Konishi, S. Hattori, H. Matsukuma, M. Murakami, S. Shimizu, and S. Tokita, "Fluoride-fiber-based side-pump coupler for high-power fiber lasers at 2.8 μm," Opt. Lett. **43**(10), 2340-2343 (2018).
25. S. Tokita, M. Murakami, and S. Shimizu, "High power 3 μm erbium fiber lasers," Advanced Solid State Lasers, paper AM3A.4 (2014).
26. Y. O. Aydin, F. Maes, V. Fortin, S. T. Bah, R. Vallée, and M. Bernier, "Endcapping of high-power 3 μm fiber lasers," Opt. Express **27**(15), 20659-20669 (2019).
27. H. Okamoto, K. Kasuga, and Y. Kubota, "Efficient 521 nm all-fiber laser: splicing $Pr^{3+}$-doped ZBLAN fiber to end-coated silica fiber," Opt. Lett. **36**(8), 1470-1472 (2011).
28. Z. Zheng, D. Ouyang, J. Zhao, S. Ruan, J. Yu, C. Guo, and J. Wang, "An effective thermal splicing method to join fluoride and silica fibers for a high power regime," Chin. Phys. Lett. **32**(11), 114206 (2015).
29. A. V. Pushkin, E. A. Migal, H. Uehara, K. Goya, S. Tokita, M. P. Frolov, Y. V. Korostelin, V. I. Kozlovsky, Y. K. Skasyrsky, and F. V. Potemkin, "Compact, highly efficient, 2.1-W continuous-wave mid-infrared Fe:ZnSe coherent source, pumped by an Er:ZBLAN fiber laser," Opt. Lett. **43**(24), 5941-5944 (2018).
30. R. I. Woodward, M. R. Majewski, G. Bharathan, D. D. Hudson, A. Fuerbach, and S. D. Jackson, "Watt-level dysprosium fiber laser at 3.15 μm with 73% slope efficiency," Opt. Lett. **43**(7), 1471-1474 (2018).
31. V. Fortin, F. Jobin, M. Larose, M. Bernier, and R. Vallée, "10-W-level monolithic dysprosium-doped fiber laser at 3.24 μm," Opt. Lett. **44**(3), 491-494 (2019).
32. D. W. Chen, C. L. Fincher, T. S. Rose, F. L. Vernon, and R. A. Fields, "Diode-pumped 1-W continuous-wave Er:YAG 3-μm laser," Opt. Lett. **24**(6), 385-387 (1999).
33. H. Uehara, S. Tokita, J. Kawanaka, D. Konishi, M. Murakami, S. Shimizu, and R. Yasuhara, "Optimization of laser emission at 2.8 μm by Er:$Lu_2O_3$ ceramics" Opt. Express **26**(3), 3497-3507 (2018).